Physical mechanism of extraordinary electromagnetic transmission in dual-metallic grating structures

Chen Cheng, Jing Chen, Da-Jian Shi, Qi-Yang Wu, Fang-Fang Ren, Ji Xu, Ya-Xian Fan, Jianping Ding, and Hui-Tian Wang*
Nanjing National Laboratory of Microstructures and Department of Physics, Nanjing University, Nanjing 210093, People's Republic of China

(Received 24 February 2008; revised manuscript received 13 May 2008; published 7 August 2008)

Very recently, in a short letter [Appl. Phys. Lett. **91**, 111111 (2007)], we outlined some important results of electromagnetic transmission in dual-metallic grating structures composed of two identical single-metallic gratings with periodic subwavelength slit arrays. Here we describe and explain our theoretical study on the propagation property of the electromagnetic radiation in such structures in detail. The results manifest that the longitudinal interval and lateral displacement between the two single-metallic gratings strongly influence the electromagnetic transmission behavior in the dual-metallic grating structures. We discover some interesting phenomena such as the frequency shift and splitting of the high transmission peak, and the transmission suppression over a broad frequency region. We reveal that the coupling between the two single-metallic gratings is responsible for those phenomena. In addition, the case of oblique incidence is also explored.

DOI: 10.1103/PhysRevB.78.075406 PACS number(s): 42.79.Dj, 42.25.Bs, 78.66.Bz, 42.25.Fx

I. INTRODUCTION

Extraordinary electromagnetic (EM) transmission through metallic slab with subwavelength hole or slit arrays has become a hot realm, due to rich physics and potential applications (such as subwavelength photolithography,[1] near-field microscopy,[2] optical modulator,[3] and flat-panel display[4]), since highlighted by Ebbesen *et al.*.[5] Sharp transmission peaks were observed at wavelengths much larger than the diameter of the holes, and the transmittance could be several orders greater than that predicted by standard aperture theory.[5] This phenomenon, which is termed the extraordinary EM transmission in metallic slabs with subwavelength microstructures, has been extensively investigated in a variety of geometric configurations, with different periods, surface structures, materials, or hole shapes.[5–17] Subwavelength metallic microstructures have been proposed to develop novel photonic devices and to explore unique physical effects, such as in nonlinear optics and quantum optics.[18–22]

An effective-medium model was proposed, which can describe well the property of the EM transmission in one-dimensional metallic gratings with subwavelength slits for the far-field case.[23,24] In particular, this model is valid when the grating period is much larger than the silt width. It should be pointed out that the influence of diffracted evanescent waves is neglected in this effective-medium theory, which is acceptable in the far-field situation, because the evanescent fields decay exponentially away from the surface of the metallic slab. However, as is well known, the evanescent fields carry the fine information of the subwavelength structure, and play an important role in the guided-mode resonance inside the slits.[25] It is of great interest to the investigation on the EM transmission behavior in cascaded metallic structures composed of two or more subwavelength gratings.

If two adjacent gratings have an appropriate interval, the diffracted evanescent fields from different gratings would feel and couple with each other. Chan *et al.*[26] reported their experimental results of the transmission of infrared radiation in a kind of bilayer metallic structure, i.e., dual-metallic grating (DMG) composed of two single-metallic gratings (SMGs). The results revealed that the transmission is surprisingly high at some particular wavelengths, even when a lateral displacement L between the two SMGs forbids the direct line of sight through the whole structure. The maximum of transmission occurs when L is zero or half of the period, and the minimum occurs when L is a quarter of period.[26] Recently, we briefly reported the EM transmission behaviors in DMGs with subwavelength slit arrays.[27] It is necessary to describe and explain theoretically the extraordinary EM transmission phenomena in such a kind of structures in detail, which is the purpose of the present article. The finite-difference time-domain (FDTD) simulation results present here include not only the transmission spectra, but also the spatial distributions of magnetic field **H** and the Poynting vector **S**.

In our FDTD simulations, a mesh size about 2 nm is used and the time step is less than 0.0045 fs in order to satisfy the FDTD stability criteria (convergence). The perfectly matched layer is used at the boundaries in the z direction. The periodic boundary condition is used in the other boundaries. Two periods of the grating are included during simulation. The source used is a p-polarized plane EM wave with a Gaussian-profile broadband frequency spectrum. The transmission spectra are recorded in the far-field region.

II. NORMAL INCIDENCE

The DMG structure treated here is the same as that in Ref. 27, composed of two identical periodic SMGs. Any SMG has a period of $d=1000$ nm, a slit width of $a=100$ nm (in the x direction), and a thickness of $h=500$ nm (in the z direction). The two SMGs can be longitudinally separated by G and laterally displaced by L. The whole structure is placed in air surrounding, and the metal is silver (Ag), whose dielectric constant obeys the following lossless Drude model[27,28]

$$\varepsilon(\omega) = 1.999 - \omega_p^2/\omega^2, \tag{1}$$

where $\omega_p = 1.34639 \times 10^{16}$ Hz is the plasma angular frequency. Our FDTD simulations validate that the transmission

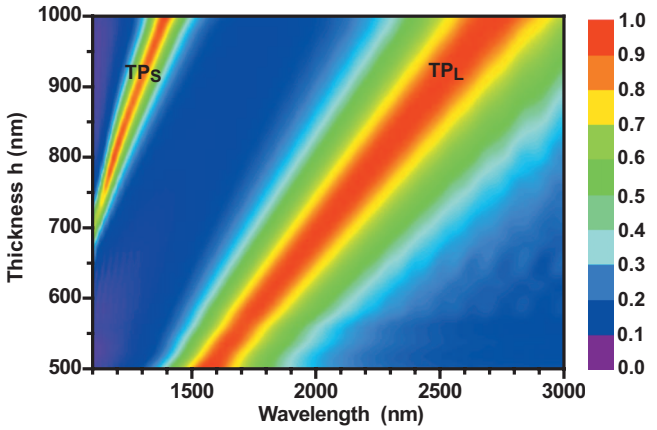

FIG. 1. (Color) Transmission spectra of the SMG structure with the thickness h ranging from 500 to 1000 nm.

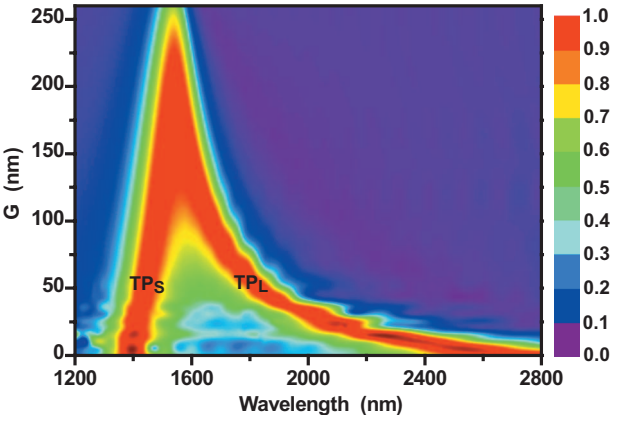

FIG. 3. (Color) Transmission spectra in the DMG structure, with the different longitudinal interval G ranging from 0 to 260 nm and without the lateral displacement $L=0$.

of the p-polarized EM radiation with the magnetic field **H** being parallel to the slits (along the y direction) is allowed only. In contrast, the s-polarized radiation can never be transmitted because the grating structures we investigated are composed of the subwavelength slits. This fact implies that the transmission in the DMG structures is associated with the surface-plasmon polariton (SPP). We thereby only investigate the p-polarized radiation in this work.

We divide this section into three subsections. In Sec. 1A, the EM transmission through SMG will be discussed. In Sec. 1B, we devote to exploring the dependence of the extraordinary EM transmission property on the longitudinal interval G in DMG, without the lateral displacement (i.e., $L=0$). Finally, in Sec. 1C, the EM transmission through DMG with both longitudinal interval and lateral displacement will be investigated. It is noted that in this section only normal incidence is explored. The oblique incidence will be briefly discussed in Sec. III.

A. In SMG structures

As a DMG contains two identical SMGs, it is necessary to investigate the EM transmission property in SMG first. SMG has been well investigated,[29–37] and the results revealed that the periodicity and thickness mainly influence the wavelength of extraordinary EM transmission peak, and the width of slit mainly influences the amplitude and linewidth of transmission peak. By changing these grating parameters, many interesting phenomena have been discovered and some important applications have been found. For example, the periodic, quasiperiodic, and aperiodic aperture structures in thick metal film possess the extraordinary transmission resonance.[30] Slits perforated in the silver slab are designed with variant widths to produce desired optical phase retardations.[31]

In the present work, the transmission spectra of SMGs are investigated for different grating thickness h ranging from 500 to 1000 nm, to seek the dependence of the wavelength of the transmission peak on the thickness h, with the goal for revealing the physical mechanism behind the extraordinary EM transmission. It should be noted that the 1000-nm-thick SMG is in fact equivalent to a DMG structure without the lateral displacement and the longitudinal interval $(L,G=0)$, i.e., the two 500-nm-thick SMGs are closely stacked together. The investigation of SMGs could provide the useful information for understanding the EM transmission behaviors in DMGs. Here we fix the grating period

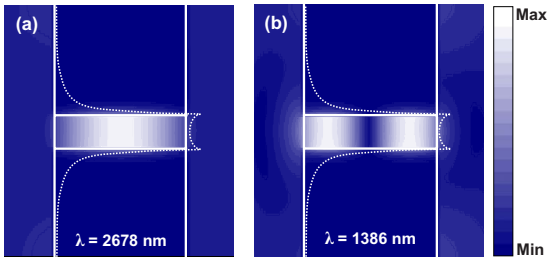

FIG. 2. (Color online) Distributions of magnetic field at the transmission peaks at (a) 2678 nm and (b) 1386 nm for a 1000-nm-thick SMG, respectively. The dotted lines are the transverse distributions of magnetic field at a half of thickness.

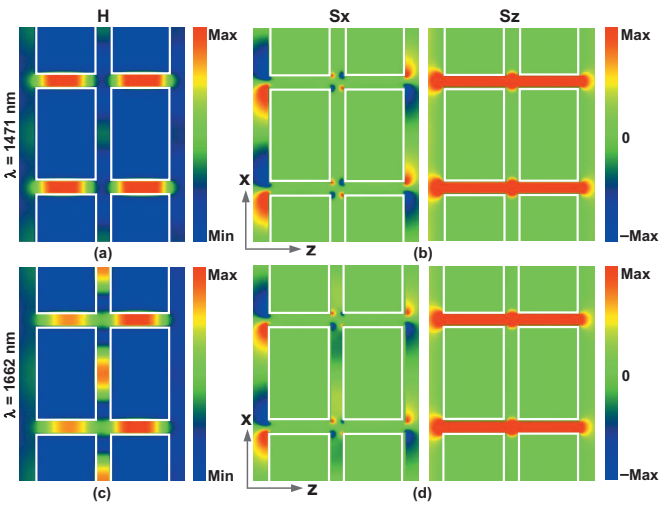

FIG. 4. (Color) Distributions of magnetic field of (a) TP_S at 1471 nm and (c) TP_L at 1662 nm for $G=100$ nm. (b) and (d) are the corresponding distributions of Poynting vector.

(d=1000 nm) and the slit width (a=100 nm) of SMG.

The calculated transmission spectrum of SMG is plotted in Fig. 1. When h=500 nm, only one extraordinary EM transmission peak (labeled as TP_L) at ~1560 nm exists. TP_L exhibits the redshift as the grating thickness h increases, and its spectral linewidth becomes broader. When h is greater than ~700 nm, the second extraordinary EM transmission peak appears in the shorter wavelength regime, which is labeled as TP_S, with the narrower spectral width than TP_L. The wavelengths of TP_L and TP_S exhibit the redshift as h further increases. It should be pointed out that there exists another narrow transmission peak at a much shorter wavelength close to the period of 1000 nm, which originates from the excitation of SPPs at both surfaces of SMG. We give a brief discussion for this short-wavelength transmission peak in the case of oblique incidence.

To reveal the physical mechanism behind the high transmission, we would like to explore the spatial distributions of magnetic field **H** at the wavelengths of TP_L and TP_S. Figures 2(a) and 2(b) depict the field distributions of TP_L at 2678 nm and TP_S at 1386 nm, respectively, for the 1000-nm-thick SMG. The magnetic field **H** in the z direction indicates the character of the Fabry-Pérot-like guided-mode resonance inside the finite-length slit.[12,27,31,38] The transverse field distribution across the slit (in the x direction), as sketched by the dotted lines in Fig. 2, has a salient feature that the field intensity at the midline of the slit is lower than that at the two Ag-air boundaries, representing the emblematical character of the symmetrically coupled-SPP modes. Therefore, the two high transmissions should be associated with the Fabry-Pérot-like guided-mode resonance of coupled-SPP modes inside the slits. Of course, the propagation behavior of the EM wave inside the slits can be indeed given by a closed-form solution.[12,31,38] According to a number of nodes inside the slits, TP_L and TP_S are related to the zeroth-order and first-order guided modes, respectively, in the 1000-nm-thick SMG.

In the present work, we devote to the DMG structures composed of two identical periodic SMGs with the grating period of d=1000 nm, the slit width of a=100 nm and the thickness of h=500 nm only, and the wavelength range we concerned is larger than the grating period. Thereby only the zeroth-order Fabry-Pérot-like coupled-SPP mode inside the slits is allowed. Of course, if the thickness of SMG is increased, higher-order modes can also be supported, which have the very similar properties with the zeroth-order mode.

B. In DMG structures without lateral displacement

After investigating the extraordinary EM transmission in the SMG structures, we now focus on the DMG structures without the lateral displacement (L=0), i.e., the two 500-nm-thick SMGs are longitudinally displaced only. The simulated transmission spectra are shown in Fig. 3 at different longitudinal separation G ranging from 0 to 260 nm.

When G=0, the DMG structure is equivalent to a 1000-nm-thick SMG. As mentioned in Sec. IA, there have two extraordinary EM transmission peaks, as TP_S at 1386 nm and TP_L at 2678 nm, which are associated with the first- and zeroth-order Fabry-Pérot-like guided-mode resonance of coupled-SPP modes inside the slits, respectively. As G increases, TP_S and TP_L move toward each other gradually, and exhibit the redshifts and blueshifts, respectively. In particular, when G is about 160 nm, TP_S and TP_L degenerate into a single transmission peak located at a wavelength of about 1550 nm, which is almost identical to that of extraordinary EM transmission in a 500-nm-thick SMG. The wavelength of this single transmission peak hardly changes when G further increases to 260 nm, while the transmittance monotonously decreases, because the two SMGs have almost decoupled.

The distributions of magnetic field **H** and Poynting vector **S** in the x and z directions are calculated. Figure 4 furnishes the simulation results for G=100 nm, at two high transmission peaks of TP_S=1471 nm and TP_L=1662 nm. Figure 5 shows the case of G=200 nm, in which only a single degenerate high transmission peak at 1550 nm exists. We can see from Figs. 4 and 5 that at these high transmission peaks, the magnetic field **H** is strongly confined inside the slits, corresponding to zeroth-order Fabry-Pérot-like guided-mode resonance of coupled-SPP modes inside the slits. For the Poynting vector **S**, one can see the EM radiation flows into the slits from the entrance and then flows out from the exit in the first SMG. Due to the coupling among the fields inside the gap, the EM radiation flows into the slits of the second SMG and then flows out. Such an EM transmission process is very similar to the "conflux" and "distributary" of water in the river. All these characters imply that any slit acts as an EM flux channel or can be termed an "EM river," and the high transmission is mediated by the Fabry-Pérot-like guided-mode resonance of coupled-SPP modes inside the slits. Noting that for TP_S and TP_L, the **H** and **S** distributions have some differences. Inside the gap, TP_L has relatively higher magnetic field **H** than TP_S and the energy flux for TP_L is also stronger (see Fig. 4). Of course, the EM field could also penetrate into the metal Ag, in which the direction of the Poynting vector **S** is opposite to that inside the slit and the gap. This opposite energy flux is confined very close to the Ag-air interface, and is difficult to be directly observed in the figures.

The distributions of magnetic field **H** and Poynting vector **S** inside the gap indicate the coupling between the two SMGs. When G is greater than 160 nm, TP_S and TP_L degenerate into a single transmission peak at ~1550 nm, which is close to the wavelength of the high transmission in a 500-nm-thick SMG (~1560 nm). The coupling is very weak in this larger gap case. When G decreases, the increase in splitting between TP_S and TP_L implies that the coupling becomes stronger. When G is zero, i.e., the two SMGs form an inseparable physical object, the coupling reaches the strongest strength, and the interval between TP_S and TP_L gets its maximum value.

It is very useful to explore what mechanism contributes to the coupling. Due to the subwavelength structure of SMGs, inside the gap, only the zeroth-order diffraction is propagating mode, while the other higher-order diffractions are evanescent fields in the z direction. Since evanescent fields decay exponentially away from the surfaces of SMGs, the propagating mode has no change in amplitude when propa-

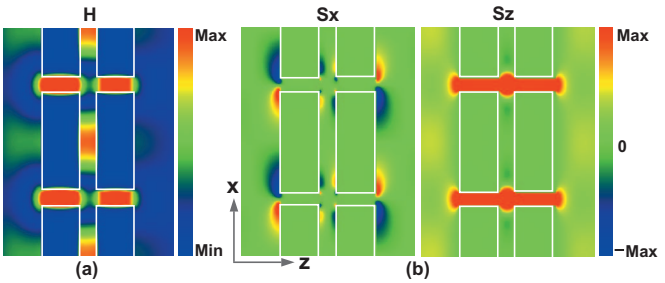

FIG. 5. (Color) (a) Distribution of magnetic field for the single transmission peak at 1550 nm for $G=200$ nm and (b) the corresponding distributions of Poynting vector.

gating in air, the increase in coupling strength with the decrease in G implies that the coupling should involve the diffracted evanescent waves. It has been proposed that the interaction of evanescent waves can influence the propagation behavior of EM radiation in the subwavelength slits.[25] So the EM transmission phenomena observed in DMGs can be understood by the interaction of evanescent waves from the subwavelength slits of two SMGs. Of course, we can understand this problem from an more intuitive physical picture. At the rear surface of the first SMG and the front surface of the second SMG, the SPP modes can be supported, respectively. When the two SMGs close with each other, the two SPP modes will couple to form a coupled-SPP mode propagating along the infinite-length gap. Based on this coupling effect, the EM radiation from the first SMG can tunnel into the second SMG through the gap. The increase in coupling strength with the decrease in G results in the splitting of the transmission peak.

The above discussions are limited within the case of $G<260$ nm. When G is further increased from 260 nm, the situation is quite different, and the calculated result is shown in Fig. 6. For instance, when $G\sim300$ nm, the transmission spectrum exhibits an unexpected transmission suppression within a broad spectral region. When G is further increased from $G=300$ nm, the high transmission emerges again. The transmission peaks can be grouped into two types. Type I is

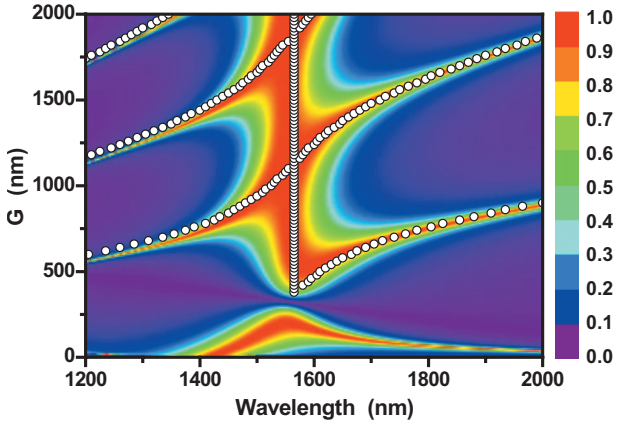

FIG. 6. (Color) Transmission spectra in the DMG structure, with the different longitudinal interval G ranging from 0 to 2000 nm and without the lateral displacement $L=0$, where the open circles are the results given by the effective-medium theory.

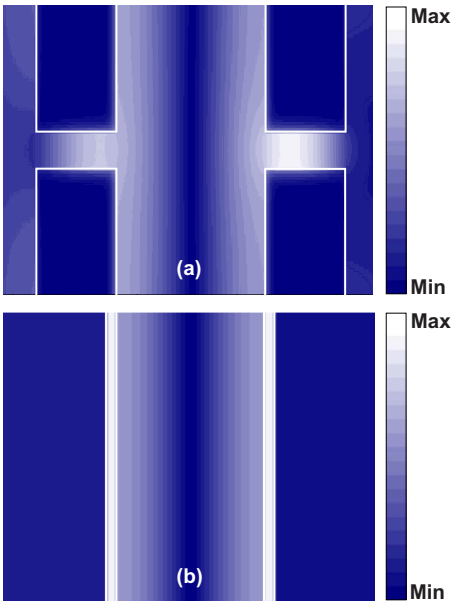

FIG. 7. (Color online) Distributions of magnetic field simulated by the FDTD method, at the wavelength of 2000 nm and with $G=900$ nm, (a) in the real DMG structure and (b) in the equivalent structure from effective-medium model with each effective-medium thickness of 78 nm.

the transmission peak that occurs always around 1560 nm. Type II includes all of other transmission peaks.

We now would like to reveal the physical mechanisms behind the Type-I and Type-II transmission peaks. For Type-I transmission peak, it is readily understood that it originates from the cascaded transmission of the Fabry-Pérot-like guided modes inside the slits in the two SMGs. For any Type-II transmission peak, it cannot be explained by the coupling effect among the evanescent fields inside the gap (or coupled-SPP mode inside the gap), due to the short propagation distance of the evanescent fields in the z direction. To get insight into the physical origin behind the Type-II peaks, the effective-medium theory pioneered in Ref. 23 might be valid. Based on the effective-medium model, the two SMGs can be equivalent to two homogeneous slabs with the same effective refractive index of d/a (=10 here) and the same

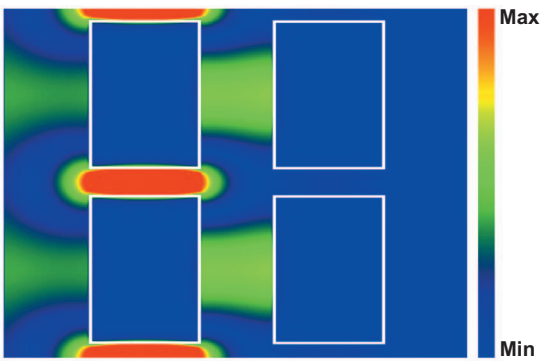

FIG. 8. (Color) Distribution of magnetic field at the wavelength of 1560 nm for $G=300$ nm, in this case, the EM transmission is suppressed.

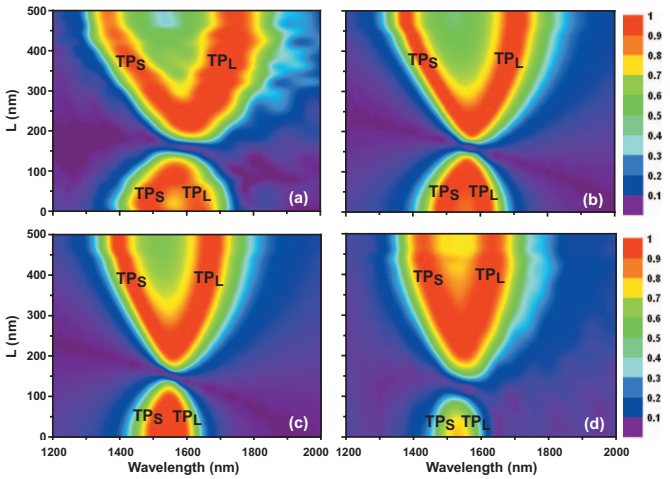

FIG. 9. (Color) Dependence of the transmission spectra on the lateral displacement L for the different longitudinal intervals G of (a) 100 nm, (b) 130 nm, (c) 160 nm, and (d) 200 nm.

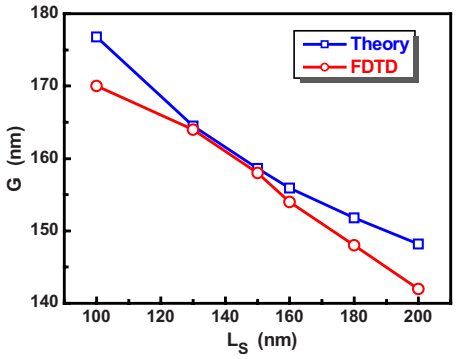

FIG. 10. (Color online) Dependence of L_S on G, where open circles and open squares are from the FDTD simulations and the theoretical model, respectively.

effective thickness of ah/d (=50 nm here), when the permittivity of the metal is large enough (or in the perfect conducting metal case). However, it seems unlikely that the effective refractive index and the effective thickness of SMG could take 10 and 50 nm here, respectively, because the two SMGs are not constructed by the perfect conducting metal. In the frame of the effective-medium model, the DMG structure with $G>300$ nm can be equivalent into a sandwich structure composed of a gap (with the refractive index $n=1$ and the thickness G) separating two equivalent slabs (with the refractive index n_{eff} and the effective thickness h_{eff}). Of course, such a sandwich structure can be considered as a multiple Fabry-Pérot cavity. Based on this model, we fit the transmission peaks calculated by the FDTD simulations, as shown in Fig. 6, and then obtain $n_{\text{eff}}=10$ nm and $h_{\text{eff}}=78$ nm. One can see that the fitted results, as shown by open circles in Fig. 6, is in good agreement with the FDTD results, suggesting that the Type-II peaks are caused by the resonance of the Fabry-Pérot cavity modes. To further recognize the physical origin behind the Type-II peaks, we compare the magnetic-field distribution of the DMG structure with the effective-medium model. As an example, Figs. 7(a) and 7(b) show the magnetic-field distributions simulated by the FDTD method in the real DMG structure and in the equivalent structure from the effective-medium model, respectively, with $G=900$ nm and at a high transmission wavelength of 2000 nm. One can see that the magnetic field inside the gap exhibits indeed the typical field distribution form of the Fabry-Pérot cavity, with a node at the midline of the gap.

To understand the transmission suppression when $G\sim300$ nm, the magnetic-field distribution is calculated, as shown in Fig. 8. The field in the entrance of each slit of the second SMG is extremely weak. Naturally, no EM radiation can flow into the slit of the second SMG, resulting in the transmission suppression. This weak-field region is due to the completely destructive interference among all orders of diffracted fields from the first SMG and their reflected fields from the second SMG. It has been proved that any single-order diffracted field and its reflected field cannot give rise to the completely destructive interference at the entrance of any slit in the second SMG.

C. In DMG structures with lateral displacement

We now investigate the situation when the two SMGs are laterally displaced, so that no direct line of sight exists between the slits.[26,27] Such an arrangement forbids directly EM propagation through the slits of the first and second SMGs, and would provide much information about the roles of the diffracted evanescent fields inside the gap.

The dependence of the transmission spectra on the lateral displacement L is explored at four different longitudinal intervals G, and the FDTD simulation results are shown in Fig. 9, in which (a), (b), (c), and (d) correspond to $G=100$, 130, 160 and 200 nm, respectively. For example, we can see from

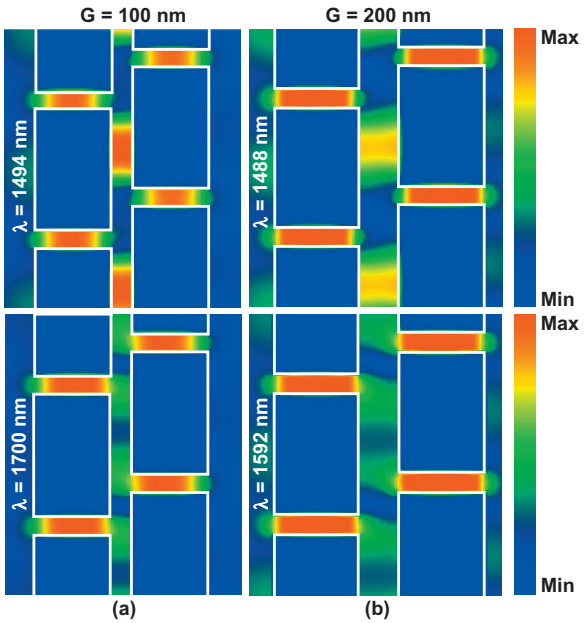

FIG. 11. (Color) Distributions of magnetic field at the transmission peaks when $L=300$. (a) $TP_S=1494$ nm and $TP_L=1700$ nm when $G=100$ nm. (b) $TP_S=1488$ nm and $TP_L=1592$ nm when $G=200$ nm.

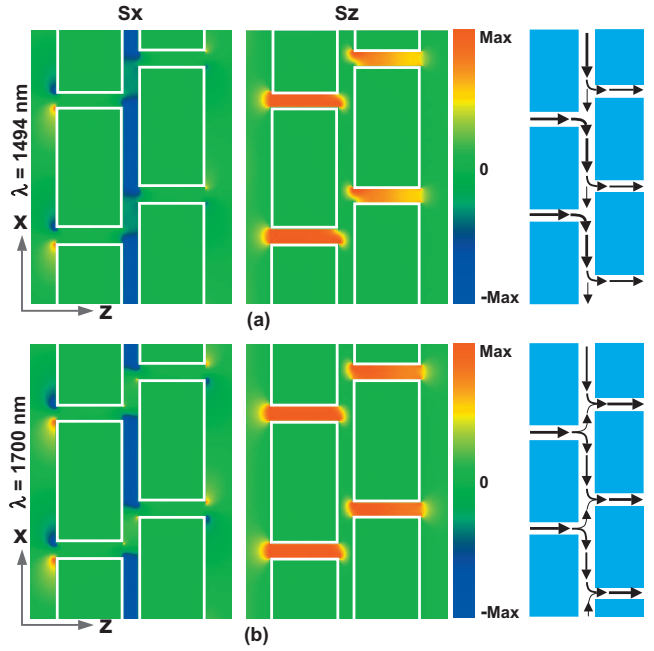

FIG. 12. (Color) Distributions of Poynting vector at the wavelength of (a) TP_S=1494 nm and (b) TP_L=1700 nm, when L=300 nm and G=100 nm. The insets in right side indicate the energy flux directions in the structure.

Fig. 9(a) that as the lateral displacement L increases from zero, the two transmission peaks TP_S and TP_L exhibit the redshifts and blueshifts, respectively, and then degenerate into a single peak at wavelength of ~1582 nm when L ~120 nm, which is very close to the wavelength of the transmission peak in the 500-nm-thick SMG. If L increases from 120 nm, the position of the single peak has almost no change while the transmittance decreases, and then when L increases to about 160 nm, the high transmission is suppressed in a broad wavelength regime and the highest transmittance decreases sharply from about 90% to 10%.[27] This suppression phenomenon is most prominent at L_S=170 nm. As L increases further, the high transmission peak emerges again at L~200 nm, and ultimately splits into two separated peaks of TP_S and TP_L if L>250 nm. The separation between TP_S and TP_L becomes greater as L increases. We can see from Fig. 9 that the phenomena as mentioned above are universal properties for different longitudinal intervals G (at

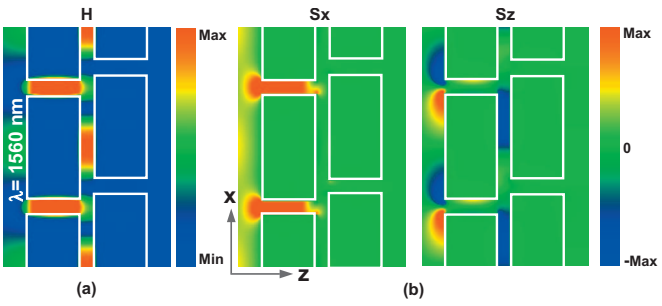

FIG. 13. (Color) Distributions of magnetic field (a) and Poynting vector (b), at the wavelength of 1560 nm when L=170 nm and G=100 nm (the EM transmission is suppressed).

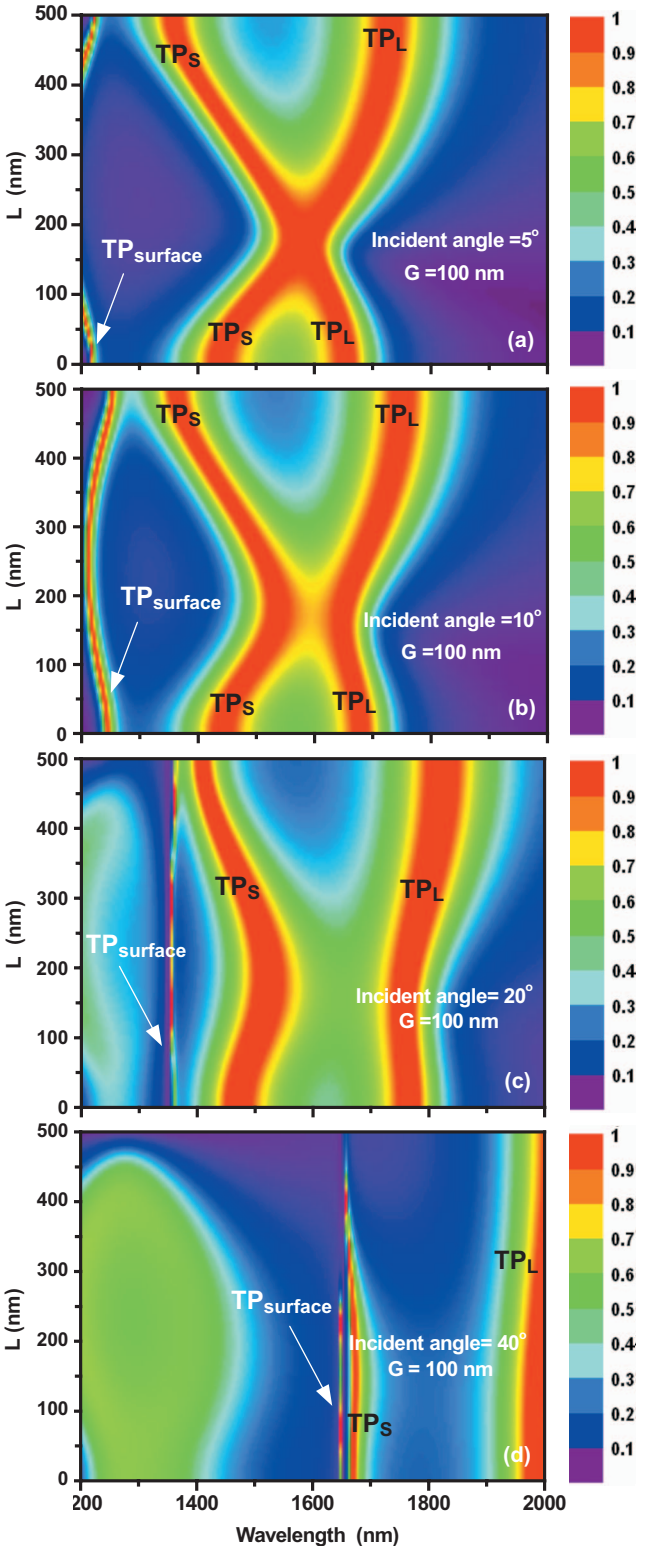

FIG. 14. (Color) Dependence of the transmission spectrum on the lateral displacement L for the different incident angles, when G=100 nm. (a) 5°, (b) 10°, (c) 20°, and (d) 40°.

least within the range of G<200 nm). For instance, when G=130 nm in Fig. 9(b), 160 nm in Fig. 9(c), and 200 nm in Fig. 9(d), the transmission suppression is also observed, which is most distinct at L_S=164, 154, and 142 nm, respec-

tively. The FDTD simulation results indicate that L_S has a decreasing tendency as G increases, as shown by circles in Fig. 10.

To understand the high transmission in detail, the distributions of the magnetic field **H** at some selected high transmission wavelengths are calculated, as shown in Fig. 11(a) for $L=300$ nm and $G=100$ nm as well as in Fig. 11(b) for $L=300$ nm and $G=200$ nm. Obviously, for all the high transmission, there is a common property that the magnetic field **H** is very strong inside the slits, as a typical behavior of the Fabry-Pérot-like guided-mode resonance of coupled-SPP modes, similar to Fig. 2(a). In contrast, the field distributions inside the gap have some differences. We can see from Fig. 11 that at the short-wavelength transmission peaks $\mathrm{TP}_S=(1494$ and 1488 nm), the magnetic field **H** is weak at the exit of each slit in the first SMG; while for the long-wavelength transmission peaks $\mathrm{TP}_L=(1700$ and 1592 nm), the magnetic field **H** is relatively strong. Distributions of Poynting vector **S** are also calculated, as an example, Fig. 12 plots the results for $\mathrm{TP}_S=1494$ nm and $\mathrm{TP}_L=1700$ nm for $L=300$ nm and $G=100$ nm, corresponding to Fig. 11(a). In Fig. 12(a) for TP_S, the direction of energy flux inside the gap is always along the $-x$ direction, while in Fig. 12(b) for TP_L, opposite energy flux can be observed inside the gap. The EM energy flux confined in the slits of the first SMG flows along the gap into the slits of the second SMG. Since a nonzero lateral displacement L forbids directly the EM propagation through two slits, the coupling of EM fields inside the gap should play an important role in the EM transmission. The coupling strength is a function of G and L. This is the reason why the EM transmission property in DMG depends not only on the longitudinal interval G but also on the lateral displacement L.

We now explore the physical mechanism behind the transmission suppression (shown in Fig. 9) in the DMG structure with the lateral displacement. Although the coupling of EM fields inside the gap can explain the splitting and shift of the transmission peak, the transmission suppression within a broad frequency range is difficult to be understood in a similar way. We calculate the distributions of magnetic field **H** and Poynting vector **S**, and the results are shown in Fig. 13 for $G=100$ nm and $L=L_S=170$ nm. Evidently, the strong EM field and the energy flux exist inside the gap and the slits of the first SMG, while there has almost no EM field and energy flux inside the slits of the second SMG.

As mentioned above, in the case of $G<260$ nm, the EM field inside the gap is the coupled-SPP mode propagating along the infinite-length gap. Such a kind of coupled-SPP mode can propagate along $+x$ or $-x$ direction inside the gap, therefore, the counter-propagating coupled-SPP modes along the infinite-length gap will certainly form a standing-wave coupled-SPP mode, based on the interference principle. As shown in Fig. 13, the entrance of each slit in the second SMG matches nicely to a node of the standing-wave coupled SPP. The most possible mechanism contributing to the transmission suppression should be the destructive interference among the counter-propagating coupled SPPs inside the gap. For the extraordinary EM transmission and the directional emission,[16] it was proposed that each opening of subwavelength metallic structures, including slits,[39] holes,[40] and grooves,[41] can be regarded as a source of coupled SPPs. In the DMG structure, the exit of each slit in the first SMG can be regarded as a source of coupled SPPs. The field at the entrance of each slit in the second SMG determines the probability of exciting the Fabry-Pérot-like coupled-SPP modes (as mentioned above) in the slits of the second SMG, which can be converted into free-space EM radiation at the rear surface of the second SMG. Due to the coupling effect between the two SMGs, the interval G will affect the propagation property of the coupled-SPP modes inside the gap. Consequently, the suppressed transmission caused by the destructive interference depends on the parameters of G and L.

We now seek the necessary condition when a node of the standing-wave coupled SPP inside the gap is nicely placed at the entrances of each slit in the second SMG. We label different slits in the first and second SMGs by the integral indices m. With the nonzero lateral displacement L, the position of the mth slit in the second SMG is between the mth and $(m+1)$th slits in the first SMG. The coupled-SPPs emitted by a pair of slits in the first SMG, the $(m-j)$th and $(m+j+1)$th slits, lead to a phase difference at the entrance of the mth slit in the second SMG, as

$$\begin{aligned}\Delta\phi(m,j) &= \{[(m+j+1)-m]d - L_S\}K_{\mathrm{eff}} \\ &\quad - \{[m-(m-j)]d + L_S\}K_{\mathrm{eff}} \\ &= (d-2L_S)K_{\mathrm{eff}}, \end{aligned} \tag{2}$$

where K_{eff} is the effective wave vector of the coupled SPP in the x direction inside the gap.[42] Clearly, $\Delta\phi(m,j)$ is independent of m and j, implying that the coupled SPPs emitted from any pair of the $(m-j)$th and $(m+j+1)$th slits in the first SMG have the identical phase difference at the entrance of the mth slit in the second SMG. Therefore, the destructive interference between the counter-propagating coupled SPPs emitted from the exits of any pair of the $(m-j)$th and $(m+j+1)$th slits in the first SMG will always occur at the entrance of the mth slit in the second SMG, provided that

$$\Delta\phi(m,j) = (d-2L_S)K_{\mathrm{eff}} = (2p+1)\pi, \tag{3}$$

where p is an integer. Here we use the dispersion relation of the coupled-SPP mode in a metal-dielectric-metal structure with the smooth interfaces[42] to approximately determine K_{eff} of the coupled-SPP mode propagating along the x direction inside the gap in the DMG structure, as follows

$$(\varepsilon_m\beta - \varepsilon_d\gamma)\exp(-\beta G) = \varepsilon_m\beta + \varepsilon_d\gamma, \tag{4}$$

where ε_d and ε_m are the permittivity of the dielectric (air) and the metal (Ag), $\beta=\sqrt{K_{\mathrm{eff}}^2-\varepsilon_d k_0^2}$ and $\gamma=\sqrt{K_{\mathrm{eff}}^2-\varepsilon_m k_0^2}$, $k_0=2\pi/\lambda$ is the wave vector in vacuum, respectively. For the concerned case here, p in Eq. (3) can take $p=0$ only, so L_S is determined by

$$L_S = (d-\pi/K_{\mathrm{eff}})/2. \tag{5}$$

Thus the dependence of L_S on G is easily calculated by Eqs. (4) and (5), and the results are plotted by the squares in Fig. 10. Evidently, the theoretical results are in good agreement with the FDTD simulations, although Eq. (4) is imprecise for treating our problem (because the two boundaries of

the gap are not smooth surfaces). Therefore, the destructive interference of counter-propagating coupled-SPP modes inside the gap may be the most responsible mechanism for the transmission suppression.

III. OBLIQUE INCIDENCE

We also simulate the dependence of the transmission spectrum on the lateral displacement L for three incident angles of 5°, 10°, 20°, and 40°, respectively, at $G=100$ nm. The calculated results are shown in Figs. 14(a)–14(d). As the incident angle increases, the transmission behavior at around $L=150$ nm will experience an evolution from transmission suppression to the appearance of single peak, and to the splitting of peak. The essential difference of the oblique incidence from the normal incidence is the disappearance of the transmission suppression around $L=150$ nm. The physical origin can be still understood by the interference effect of the coupled-SPP modes inside the gap. Referencing to the case of normal incidence in Sec. II, in the case of oblique incidence, the coupled SPPs emitted by a pair of slits in the first SMG, the $(m-j)$th and $(m+j+1)$th slits, lead to a phase difference at the entrance of the mth slit in the second SMG, as follows

$$\begin{aligned}\Delta\phi_{ob}(m,j) &= \{[(m+j+1)-m]d - L_S\}K_{\text{eff}} \\ &\quad - \{[m-(m-j)]d + L_S\}K_{\text{eff}} + (2j+1)dk_0 \sin\theta \\ &= (d-2L_S)K_{\text{eff}} + (2j+1)dk_0 \sin\theta, \end{aligned} \tag{6}$$

where the term of $(2j+1)dk_0 \sin\theta$ is an additional phase caused by the oblique incidence with an incident angle of θ. Clearly, the phase difference depends on j while is independent of m. If assuming the phase difference of the coupled SPPs emitted from the two most adjacent slits in the first SMG with respect to the mth slit in the second SMG, $\Delta\phi_{\text{ob}}(m,0)=(d-2L_S)K_{\text{eff}}+dk_0 \sin\theta$ when $j=0$; to be π, it is difficult to make $\Delta\phi_{\text{ob}}(m,j)$ for any j be π or $(2p+1)\pi$ simultaneously. We thereby can never expect that all $\Delta\phi_{\text{ob}}(m,j)$ for any j are in phase and equal to π or $(2p+1)\pi$. Inasmuch as the perfect destructive interference is forbidden, the transmission suppression phenomenon disappears under the oblique incidence. We also find that the transmission peaks (both TP_S and TP_L) exhibit the redshift as the incident angle increases, as shown in Fig. 14. Moreover, when the incident angle is large enough, the lateral displacement has weak influence on TP_S and TP_L in the transmission spectrum, unlike in the situation of smaller incident angle.

In addition, in the short-wavelength region, a narrow transmission peak is also observed, as shown in Fig. 14. As is well known, such a transmission peak is caused by the excitation of surface resonance mode of SPPs,[5–7] which is labeled as $\text{TP}_{\text{surface}}$. The $\text{TP}_{\text{surface}}$ curve has the bowlike shape and exhibits the symmetry about $L=d/4=250$ nm, which implies that $\text{TP}_{\text{surface}}$ is influenced by the lateral displacement. In the case of larger incident angle, the $\text{TP}_{\text{surface}}$ curve becomes a nearly straight line, suggesting that the lateral displacement has almost no influence on $\text{TP}_{\text{surface}}$. As the incident angle increases, $\text{TP}_{\text{surface}}$ exhibits the redshift moving faster than that of TP_S and TP_L. When the incident angle is very large, for instance, as shown in Fig. 14(d), the part of TP_S has been swallowed down by $\text{TP}_{\text{surface}}$. In particular, when the incident angle is large enough, TP_S will completely disappear due to the strong interaction between SPP and Fabry-Pérot resonances at large angles.[6]

IV. CONCLUSION

We devote to investigating the EM transmission property of the DMG structures composed of two identical SMGs with the periodic subwavelength slit array in detail. Using the FDTD method, we calculate the transmission spectra, the distributions of magnetic field **H** and Poynting vector **S**, for different lateral displacements and longitudinal intervals between the two SMGs under the normal incidence. Some interesting phenomena are found, including the frequency shift and splitting of transmission peak as well as the transmission suppression within a broad spectral region. The physical mechanisms behind these phenomena are revealed. In addition, under the oblique incidence, we explore the EM transmission property of the DMG structures, and discover the disappearance of the transmission suppression phenomenon and recognize its physical origin.

These interesting properties make the DMG structures may be a kind of promising important photonic elements in future nanophotonic systems. The DMG structures have some advantages with respect to the SMG structures. For example, the transmission peak of a SMG is very sensitive to any parameter (such as period and slit width) fluctuations that are unavoidable in practical fabrication. Once a SMG is fabricated, it is difficult to tune the wavelength of high-transmission peak. However, if the DMG structure is used, the transmission window can be easily controlled by tuning the lateral displacement or/and longitudinal interval between the two SMGs. The transmission wavelength of the DMG structure can be precisely adjusted before solidified into a photonic circuit or chip.

ACKNOWLEDGMENTS

This work is partly supported by the State Key Program for Basic Research of China under Grant No. 2006CB921805, by the 111 project under Grant No. B07026, and by the Key Program of Ministry of Education of People's Republic of China under Grant No. 305007.

*htwang@nju.edu.cn

[1] X. G. Luo and T. Ishihara, Appl. Phys. Lett. **84**, 4780 (2004).
[2] J. Zhang, C. W. See, M. G. Somekh, M. C. Pitter, and S. G. Liu, Appl. Phys. Lett. **85**, 5451 (2004).
[3] A. L. Lereu, A. Passian, J. P. Goudonnet, T. Thundat, and T. L. Ferrell, Appl. Phys. Lett. **86**, 154101 (2005).
[4] N. Fang, H. Lee, C. Sun, and X. Zhang, Science **308**, 534 (2005).
[5] T. W. Ebbesen, H. J. Lezec, H. F. Ghaemi, T. Thio, and P. A. Wolff, Nature (London) **391**, 667 (1998).
[6] J. A. Porto, F. J. García-Vidal, and J. B. Pendry, Phys. Rev. Lett. **83**, 2845 (1999).
[7] F. J. García-Vidal, H. J. Lezec, T. W. Ebbesen, and L. Martín-Moreno, Phys. Rev. Lett. **90**, 213901 (2003).
[8] D. E. Grupp, H. J. Lezec, T. W. Ebbesen, K. M. Pellerin, and T. Thio, Appl. Phys. Lett. **77**, 1569 (2000).
[9] L. Martín-Moreno, F. J. García-Vidal, H. J. Lezec, K. M. Pellerin, T. Thio, J. B. Pendry, and T. W. Ebbesen, Phys. Rev. Lett. **86**, 1114 (2001).
[10] K. J. Klein Koerkamp, S. Enoch, F. B. Segerink, N. F. van Hulst, and L. Kuipers, Phys. Rev. Lett. **92**, 183901 (2004).
[11] K. L. van der Molen, K. J. Klein Koerkamp, S. Enoch, F. B. Segerink, N. F. van Hulst, and L. Kuipers, Phys. Rev. B **72**, 045421 (2005).
[12] Y. Takakura, Phys. Rev. Lett. **86**, 5601 (2001).
[13] R. Gordon, Phys. Rev. B **73**, 153405 (2006).
[14] H. J. Lezec, A. Degiron, E. Devaux, R. A. Linke, L. Martín-Moreno, F. J. García-Vidal, and T. W. Ebbesen, Science **297**, 820 (2002).
[15] H. F. Ghaemi, T. Thio, D. E. Grupp, T. W. Ebbesen, and H. J. Lezec, Phys. Rev. B **58**, 6779 (1998).
[16] L. Martín-Moreno, F. J. García-Vidal, H. J. Lezec, A. Degiron, and T. W. Ebbesen, Phys. Rev. Lett. **90**, 167401 (2003).
[17] L. Yin, V. K. Vlasko-Vlasov, A. Rydh, J. Pearson, U. Welp, S. H. Chang, S. K. Gray, G. C. Schatz, D. B. Brown, and C. W. Kimball, Appl. Phys. Lett. **85**, 467 (2004).
[18] H. Shin and S. Fan, Phys. Rev. Lett. **96**, 073907 (2006).
[19] W. L. Barnes, A. Dereux, and T. W. Ebbesen, Nature (London) **424**, 824 (2003).
[20] P. R. Villeneuve, Phys. World **11**, 28 (1998).
[21] E. Altewischer, M. P. van Exter, and J. P. Woerdman, Nature (London) **418**, 304 (2002).
[22] I. I. Smolyaninov, A. V. Zayats, A. Gungor, and C. C. Davis, Phys. Rev. Lett. **88**, 187402 (2002).
[23] J. T. Shen, P. B. Catrysse, and S. H. Fan, Phys. Rev. Lett. **94**, 197401 (2005).
[24] J. Shin, J. T. Shen, P. B. Catrysse, and S. H. Fan, IEEE J. Sel. Top. Quantum Electron. **12**, 1116 (2006).
[25] B. Hou, J. Mei, M. Z. Ke, W. J. Wen, Z. Y. Liu, J. Shi, and P. Sheng, Phys. Rev. B **76**, 054303 (2007).
[26] H. B. Chan, Z. Marcet, Kwangje Woo, D. B. Tanner, D. W. Carr, J. E. Bower, R. A. Cirelli, E. Ferry, F. Klemens, J. Miner, C. S. Pai, and J. A. Taylor, Opt. Lett. **31**, 516 (2006).
[27] C. Cheng, J. Chen, Q. Y. Wu, F. F. Ren, J. Xu, Y. X. Fan, and H. T. Wang, Appl. Phys. Lett. **91**, 111111 (2007).
[28] M. I. Markovic and A. D. Rakic, Appl. Opt. **29**, 3479 (1990); OPTIFDTD, Version 5.0, Technical Background and Tutorials, Optiwave Co.
[29] Q. R. Xing, S. X. Li, Z. Tian, D. Liang, N. Zhang, L. Y. Lang, L. Chai, and Q. Y. Wang, Appl. Phys. Lett. **89**, 041107 (2006).
[30] T. Matsui, A. Agrawal, A. Nahata, and Z. V. Vardeny, Nature (London) **446**, 517 (2007).
[31] T. Xu, C. L. Du, C. T. Wang, and X. G. Luo, Appl. Phys. Lett. **91**, 201501 (2007).
[32] F. J. García-Vidal and L. Martín-Moreno, Phys. Rev. B **66**, 155412 (2002).
[33] Z. J. Sun, Y. S. Jung, and H. K. Kim, Appl. Phys. Lett. **83**, 3021 (2003).
[34] H. F. Shi, C. T. Wang, C. L. Du, X. G. Luo, X. C. Dong, and H. T. Gao, Opt. Express **13**, 6815 (2005).
[35] C. T. Wang, C. L. Du, and X. G. Luo, Phys. Rev. B **74**, 245403 (2006).
[36] I. Avrutsky, Y. Zhao, and V. Kochergin, Opt. Lett. **25**, 595 (2000).
[37] A. P. Hibbins, I. R. Hooper, M. J. Lockyear, and J. R. Sambles, Phys. Rev. Lett. **96**, 257402 (2006).
[38] A. P. Hibbins, M. J. Lockyear, and J. R. Sambles, J. Appl. Phys. **99**, 124903 (2006).
[39] P. Lalanne, J. P. Hugonin, and J. C. Rodier, Phys. Rev. Lett. **95**, 263902 (2005).
[40] Z. C. Ruan and M. Qiu, Phys. Rev. Lett. **96**, 233901 (2006).
[41] F. J. García-Vidal, L. Martín-Moreno, H. J. Lezec, and T. W. Ebbesen, Appl. Phys. Lett. **83**, 4500 (2003).
[42] E. N. Economou, Phys. Rev. **182**, 539 (1969).